Journal of Materials Science: Materials in Electronics (2018) 29:16639–16646
https://doi.org/10.1007/s10854-018-9756-y

Synthesis, characterization, resistivity and magnetoresistance of $Ba_2Fe_{1-x}Ga_xMoO_6$ double perovskite

Y. Markandeya[1] · Y. Suresh Reddy[2] · S. Varaprasad[3] · K. Suresh[4] · G. Bhikshamaiah[2]

Received: 18 March 2018 / Accepted: 26 July 2018 / Published online: 14 August 2018

Abstract
Effect of Ga addition on structure, resistivity and magnetoresistance of $Ba_2Fe_{1-x}Ga_xMoO_6$ (x = 0.0, 0.1, 0.25 and 0.3) double perovskite. The sol–gel procedure was used to synthesize $Ba_2Fe_{1-x}Ga_xMoO_6$ double perovskite and consolidated at 1150 °C under Ar/H_2 atmosphere. Single phase with cubic crystal structure confirmed for all the samples through X-ray diffraction studies. Variation of grain size behavior on the samples surface has been studied by scanning electron microscopy (SEM). The spectra from energy dispersive X-ray spectroscopy (EDS) showed that all the elements Ba, Fe, Ga, Mo and O are present in the samples and there are no impurities in the materials. Fourier transform infrared spectroscopy (FTIR) spectral analysis of samples produced three characteristic absorption bands of Mo–O and Fe–O vibrations in the wave number range 400–1000 cm^{-1} which confirmed the present materials are double perovskite phase. Magneto-resistance (MR %) of these samples reduce with the addition of Ga content at room temperature (RT). Whereas, MR% at 5 K exhibits opposite trend to the MR% at RT with the Ga-content. It is found that all samples show semiconductor behavior at 5 K and changes into metallic nature as temperature increases showing a semiconductor-metallic transition. This value is larger for composition x = 0.3 and smaller for parent compound.

1 Introduction

Room temperature negative colossal magneto-resistance at the low magnetic field observed in polycrystalline ordered double type perovskite Sr_2FeMoO_6 oxides in 1998 [1]. Since then, these classes of materials greatly attracted researcher for the fundamental and technological importance [1–5]. Typically, the double perovskite oxides have the formula unit $A_2BB'O_6$, where A (Sr, Ba, Ca), B (Fe) and B′ (Mo, Re, W) are the metal ions of +2, +3 and +5, respectively. These double perovskites possess the tetragonal or the cubic crystal structure with a space group symmetry of *I4/mmm*, or $Fm\bar{3}m$ depends upon chemistry or doping, respectively [6–8]. It is reported that huge low field magnetoresistance (LFMR) at room temperature in double perovskite compound owing to the spin dependent scattering of electrons at the magnetic domain boundaries or the grain boundaries extend to inter grain tunneling effect [1, 9]. This inter grain tunneling arises due to insulating grain boundaries where the charge carrier electrons are spin-polarized [10, 11]. Double perovskite A_2FeMoO_6 have an ordered structure, which consists of alternating MoO_6 and FeO_6 octahedra along the axis of the crystal, while the voids in between the octahedral are occupied by 'A' cation [1, 12]. Double perovskite A_2FeMoO_6 exhibits metallic and ferrimagnetic properties below Curie temperature (T_c). The phenomena had been explained using the antiferromagnetic coupling between the itinerant down spin $Mo^{+5}(4d^1)$ and the localized up spin $Fe^{3+}(3d^5)$, due to this magnetic structure of double perovskite, saturation magnetization (M_s) of 4 μB per formula achieved theoretically in the ferrimagnetic state [13]. However, the observed value of M_s is lower than the reported value [1, 14]. The less value of M_s is due to ascribed to the mixed site (or lattice site) disorder between Mo and Fe ions [1, 15].

Replacement of Ba atom to Sr in $(Sr_{1-x}Ba_x)_2FeMoO_6$ compound results in enhanced saturation magnetization

✉ Y. Markandeya
markphysics@gmail.com

1 Department of Physics, Nizam College, Osmania University, Hyderabad 500 001, India

2 Department of Physics, Osmania University, Hyderabad 500 007, India

3 Department of Physics, JNTUA, Ananthapuramu 515 002, India

4 International Advanced Research Centre for Powder Metallurgy and New Materials (ARCI), Hyderabad 500 005, India

whereas the Curie temperature is reduced. The saturation magnetization and Curie temperature of the Sr_2FeMoO_6 and Ba_2FeMoO_6 compound are 3.45 and 3.70 μ_B/f.u., 420–450 and 320–340 K, respectively [2, 10–13, 16–25]. The MR% at 7 T and 330 K for the Ba_2FeMoO_6 compound is 15% [2] which is double than that of Sr_2FeMoO_6 compound [1]. Therefore, the Ba contained double perovskite exhibits improved compare magnetic properties to Sr_2FeMoO_6. Further doping of the +3 ions at B or B′ site of the $A_2BB'O_6$ double perovskite may produce further enhanced magnetic and magnetoresistance properties of Ba_2FeMoO_6 compound. Lu et al. [26] reported that improved magnetoresistance of $Sr_2Fe_{1-x}Ga_xMoO_6$ compound with Ga addition. It is interesting to investigate the effect of Ga ions replacement for the Fe in Ba_2FeMoO_6 compound on the transport and magnetoresistance properties. Therefore, we have investigated transport and magnetoresistance properties with the Ga concentration in $Ba_2Fe_{1-x}Ga_xMoO_6$ (x = 0.0, 0.1, 0.25, and 0.3) compounds, which are synthesized by sol–gel method. Further these materials were aslo characterized by XRD, SEM, EDS and FTIR.

2 Experimental

Double perovskite of $Ba_2Fe_{1-x}Ga_xMoO_6$ (x = 0.0, 0.1, 0.25 and 0.3) (BFGMO) samples were prepared by sol–gel procedure by talking stoichiometric ratio of $Ba(NO_3)_2$, $Fe(NO_3)_3 9H_2O$, $Ga(NO_3)_3$ and H_2MoO_4 (Analytical Reagent grade from Aldrich). Details of sample (sol–gel) preparation were reported [27–36]. The powders of BFGMO samples were pelletized into dimensions 1 cm dia and about 2 mm thick using harden steel dies and a hydraulic press at 2 ton m^{-2}. These pellets were sintered at 1200 °C for 6 h. To reduce Mo^{6+} to Mo^{5+}, samples were subjected to heat-treated at 1150 °C for 3 h under partial hydrogen (10% H_2 + 90% Ar). Phase purity, lattice parameter and crystal structure were evaluated using the X-ray diffraction (XRD) technique. XRD profiles of the samples were collected using Philips PW-1830 (40kV × 25 mA) with Cu-Kα radiation in step mode with a step width (2θ) of 0.02° and time of 0.5 s in the range between of 20° and 80°. The surface morphology and micro structural studies of these double perovskites were analyzed using the SEM with (Model No. Joel JSM 5600) combined micro analyzer. The elemental analysis of the BFGMO was determined by EDS (Model: OXFORD). These materials were analyzed using FTIR by Bruker Tensor 27 DTGS TEC detector spectrophotometer in the wave number range 400–1000 cm^{-1} by the KBr pellet method.

Electrical resistivity measurements were carried out by the standard four-probe method in the temperature range 5–300 K at the constant magnetic field of 0 and 5 T using laboratory-made resistivity meter that inserts along with OXFORD superconducting magnet system. Electrical resistivity data were also collected at constant temperature 5 and 300 K by varying the magnetic field from 0 to 8 T. MR (%) of the samples was calculated using this resistivity data as a function of magnetic field as well as the temperature.

Table 1 The values of lattice parameter (a), unit cell volume (V) and tolerance factor (t) of $Ba_2Fe_{1-x}Ga_xMoO_6$ (x = 0.0, 0.1, 0.25 and 0.3) double perovskite samples

Composition (x)	0	0.1	0.25	0.3
a[Å]	8.073	8.056	8.037	8.011
V[$(Å)^3$]	526.14	522.83	519.18	514.12
t	0.9627	0.9633	0.9642	0.9645

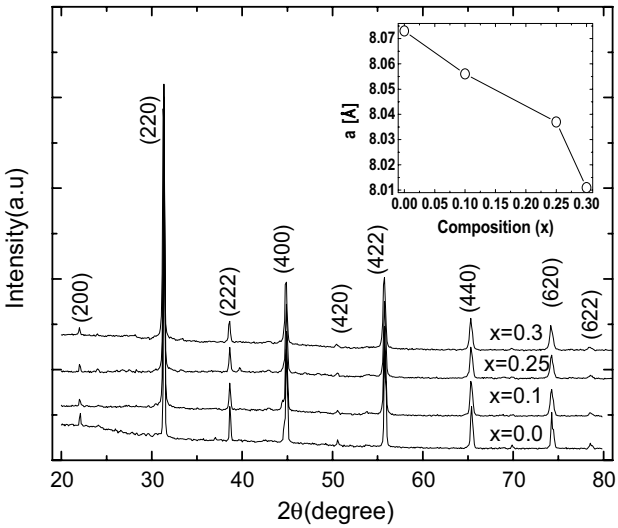

Fig. 1 X-ray diffraction pattern of $Ba_2Fe_{1-x}Ga_xMoO_6$ (x = 0.0, 0.1, 0.25 and 0.3) samples at room temperature

3 Results and discussion

3.1 Characterization

Figure 1 shows the XRD profiles of BFGMO samples at temperature 300 K. The X-ray pattern of all the samples reveals the single phase double perovskite structure of Ba_2FeMoO_6 with cubic crystal structure having space group of $Fm\bar{3}m$ [7, 9, 13, 22, 33, 34, 37, 38]. The lattice parameter 'a' and volume of unit cell 'V' of individual samples in BFGMO series were evaluated using Bragg's angle with the corresponding (*hkl*) which are in Table 1. Lattice parameter decreases with Ga concertation, inset to Fig. 1. It is evident that the considerable reduction of lattice parameter and unit cell volume

arises due to the replacement of the smaller Ga^{3+} (0.62 Å) ions in the Fe^{3+} (0.645 Å) ionic sites [39, 40], which obeys the Vegard's law [41]. JCPDS card no. 01-083-3584 was used to index XRD profile of the $Ba_2Fe_{1-x}Ga_xMoO_6$ double perovskite. Estimated crystallite (diffracted domain) size from the XRD profiles for all the samples using peak broadening (Williamson-Hall) method are above 150–280 nm due to very small value of full width half maxima (FWHM) of 0.112°–0.0876°, which are very close to instrumental broadening of 0.058° for the 2θ of 31.34°.

The tolerance factor (t) is a semi-quantitative estimation of double perovskite to know the closeness of cubic structure and its stability. The tolerance factor (t) adopted to $A_2B_{(1-x)}B''_xB'O_6$ double perovskite [26, 31, 34, 38, 42] given by

$$t = \frac{r_A + r_O}{\sqrt{2}\left(\frac{r_B(1-x)}{2} + \frac{r_{B''}x}{2} + \frac{r_{B'}}{2} + r_O\right)} \quad (1)$$

where r_A, r_B, $r_{B''}$, $r_{B'}$ and r_O are ionic radii of the respective ions [43]. They calculated tolerance factor of $Sr_2Fe_{1-x}Ga_xMoO_6$ using Eq. (1) and symmetry of lattice was described. In this investigation, the value tolerance factor (t) for $Ba_2Fe_{1-x}Ga_xMoO_6$ samples were evaluated by using Eq. (1) and the values are given in Table 1. It is observed that the tolerance factor (t) rises towards the unity with increase of Ga content in BFGMO samples owing to lowering of distortion from double perovskite structure [26, 44]. Thus symmetric nature of the present double perovskite compounds increases due to the substitution of Ga at Fe-site in Ba_2FeMoO_6.

The FE-SEM secondary electron images of BFGMO samples observed from freshly cleaved surfaces are shown in Fig. 2. Cleaved surfaces of all these samples exhibits well grown faceted grains with size of above 1 μm. Energy dispersive spectra's (EDS) of BFGMO samples are shown in Fig. 3. The results from EDS analysis showed that the elements Ba, Fe, Ga, Mo and O are present and no other impurities exists in the present samples. Measured chemical compositions of BFGMO samples are given Table 2.

Figure 4 shows FTIR spectra of the BFGMO samples in the spectral wave number range 1000–400 cm^{-1} at room temperature. The FTIR spectra of the perovskite structure have three characteristic absorption bands between 850 and 400 cm^{-1}, respective to composition and these are usually used to identify the perovskite phase formation [32, 35, 36, 45]. From the FTIR spectra of the BFGMO samples investigated in the present study, three bands for Fe and Mo are detected. These bands are, one strong band

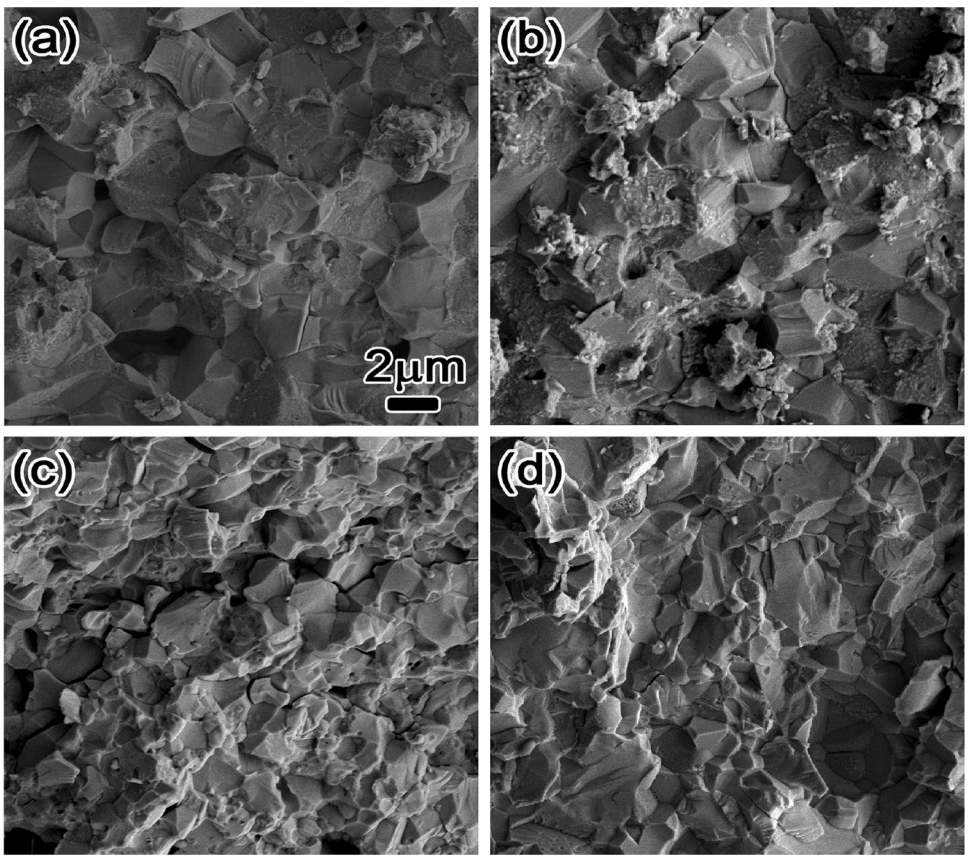

Fig. 2 (**a**–**d**) Scanning electron microscopy photographs of $Ba_2Fe_{1-x}Ga_xMoO_6$ samples for composition (**a**) x = 0.0, (**b**) x = 0.1, (**c**) x = 0.25 and (**d**) x = 0.3

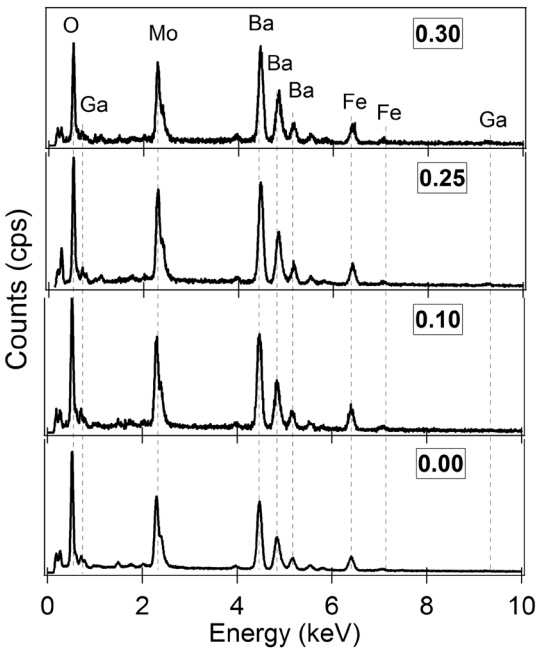

Fig. 3 Energy dispersive X-ray spectrograph of $Ba_2Fe_{1-x}Ga_xMoO_6$ samples for composition x = 0.0, 0.1, 0.25 and 0.3

in the high wave number range (~ 824 cm^{-1}) associated to the Mo–O symmetric stretching mode of MoO_6-octahedra, another band at ~ 654 cm^{-1} assigned to the anti-symmetric stretching mode of the MoO_6-octahedra, due to the higher charge of this cation [32, 35, 36, 46]. In BFGMO double perovskite, the highly charge Mo^{5+} cation octahedra, the MoO_6, act as independent groups, the vibration spectrum therefore arises from such MoO_6-octahedra. Mo–O symmetric stretching mode of MoO_6-octahedra at about 824 cm^{-1} is usually an infrared inactive vibration, but in double perovskite, both Fe and Mo ions exist in Fe and Mo sites, it becomes partially allowed due to lowering site symmetry [32, 35, 36, 46]. One more weak absorption band at about 498 cm^{-1} is ascribed to Fe–O vibration absorption of FeO_6-octahedra. For all the samples, these bands confirm the formation of perovskite phase.

3.2 Electrical resistivity

Temperature dependent electrical resistivity (ρ) at constant magnetic fields of 0 and 5 T are shown in Fig. 5a–d. The resistivity of all compositions at low temperature decreases with the increase of temperature, and a further increase of temperature at a certain point, called transition temperature, resistivity starts increasing, which infers that all samples at low temperature behave like semiconductor and after transition temperature behaves like metal. Since all the BFGMO samples behaved like as semiconductor and metallic at lower and higher temperature regimes, respectively [26, 27, 30, 38, 39, 47–50] a semiconductor to metallic transition (T_{SM}) occurs in this BFGMO series. The T_{SM}'s are obtained from Fig. 5a–d which are given in Table 3. It is known from Table 3 that T_{SM} is high for composition x = 0.3 and low for composition x = 0.0 since resistivity is greater and smaller, respectively in BFGMO samples. The T_{SM} decreases with the increase of magnetic field in BFGMO samples, which might be due to a decrease in resistivity with a magnetic field. It is shown from Fig. 5a–d that with change in Ga-content in BFGMO, there is no systematic variation of resistivity which may be due to disorder in the grain boundaries which vary randomly in the samples [33, 49, 51]. Higher resistivity values of Ga-containing samples than parent compound Ba_2FeMoO_6 may be due to larger grain boundaries [9]. It may also be expected that Ga^{3+} acts as a barrier to electron transport, reducing the number of pathways for electron percolation [30, 47, 49, 52].

The magnetic field dependence of electrical resistivity (ρ) of BFGMO samples in the magnetic field range 0–8 T keeping temperatures constant at 5 and 300 K are shown in Figs. 6a–d and 7a–d respectively. It is seen from Figures that the resistivity of BFGMO samples decreases with increase of magnetic field at temperatures 5 and 300 K. The decrease in resistivity may be due to increase of magnetic ordering with magnetic field which in turn reduces electron-magnon scattering [30, 53].

Table 2 Theoretical (Theor) and Experimental (Exp) values of Weight (%) of elements (Ba, Fe, Ga, Mo and O) in $Ba_2Fe_{1-x}Ga_xMoO_6$

wt (%)	Composition											
	x = 0.0			x = 0.1			x = 0.25			x = 0.3		
	Theor.	Exp.	Error	Theor.	Exp.	Error	Theor.	Exp.	Error	Theor.	Exp.	Error
Ba	52.57	54.46	1.89	52.43	51.93	0.5	52.23	53.84	1.61	52.16	52.64	0.48
Fe	10.69	11.61	1.08	9.60	11.82	2.22	7.96	7.60	0.36	7.42	8.03	0.61
Ga	0	0	0	1.33	0.99	0.34	3.31	2.79	0.52	3.97	3.07	0.9
Mo	18.36	18.89	0.53	18.32	19.96	1.64	18.24	20.69	2.45	18.22	20.95	2.73
O	18.37	15.04	3.33	18.32	15.30	3.02	18.25	15.08	3.17	18.22	15.31	2.91

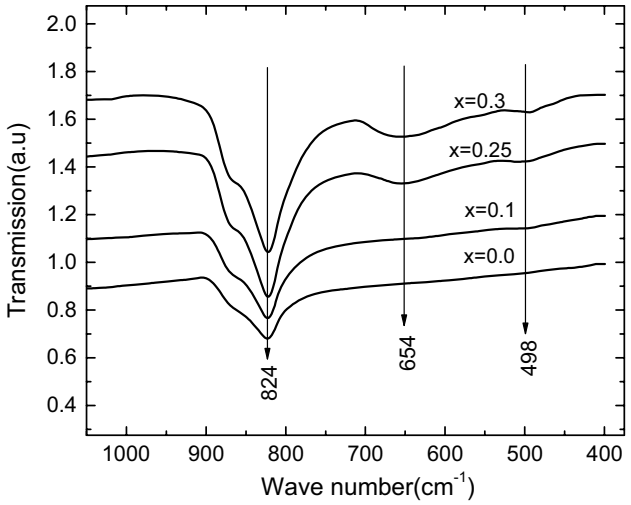

Fig. 4 FTIR spectra of $Ba_2Fe_{1-x}Ga_xMoO_6$ (x = 0.0, 0.1, 0.25 and 0.3) samples at room temperature

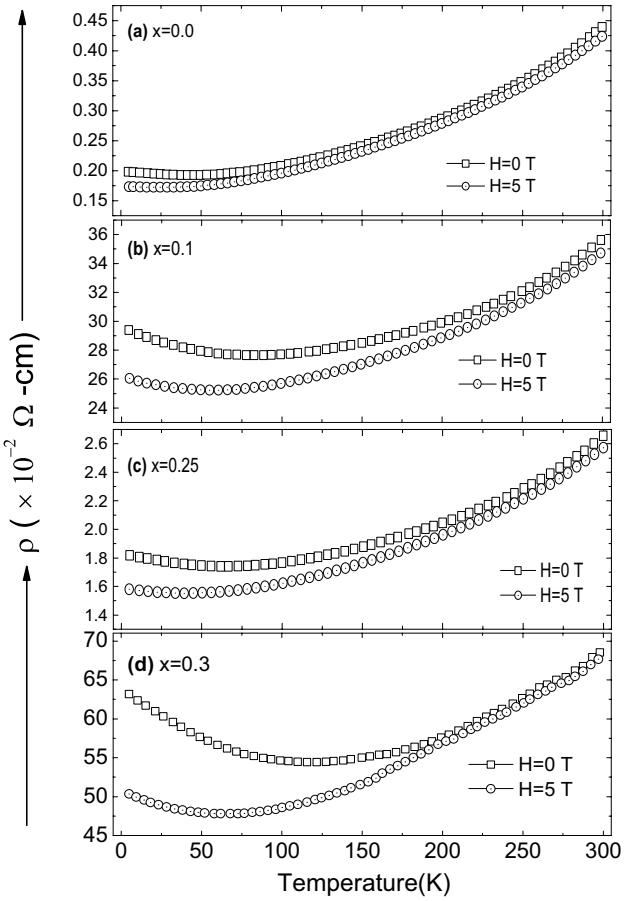

Fig. 5 (**a**–**d**) Variation of resistivity with temperature from 5 to 300 K of $Ba_2Fe_{1-x}Ga_xMoO_6$ at constant magnetic field 0 and 5 T for composition (**a**) x = 0.0, (**b**) x = 0.1, (**c**) x = 0.25 and (**d**) x = 0.3

Table 3 The values of semiconductor- metallic transition temperature (T_{SM}) and MR (%) of $Ba_2Fe_{1-x}Ga_xMoO_6$ (x = 0.0, 0.1, 0.25 and 0.3) samples

Composition (x)	0	0.1	0.25	0.3
T_{SM} (K) at 0 T	45	85	68	138
T_{SM} (K) at 5 T	27	59	44	71
MR (%) [at 5 K and 1 T]	− 5.2	− 5.1	− 5.71	− 10.62
MR (%) [at 300 K and 1 T]	− 0.77	− 0.71	− 0.75	− 0.2

3.3 Magnetoresistance

Magnetoresistance (MR%) of the material is given by

$$MR(\%) = \frac{\rho(H,T) - \rho(0,T)}{\rho(0,T)} \times 100 \quad (2)$$

where ρ(0,T) and ρ(H,T) are the resistivities at zero magnetic field and H magnetic field at temperature T respectively.

Figure 8 shows variation of MR (%) with temperature at 5 T (Tesla) for all BFGMO samples. It is observed that the variation of MR (%) increases with the decrease of temperature at the constant field of 5 T for BFGMO samples. It is well known from the literature that the grain boundary effect dominates the MR (%) as temperature decreases below Curie temperature [1, 38, 52, 54, 55]. Since grain boundary effects the MR (%) of BFGMO sample, goes to higher value as spin polarization increases with the decrease of temperature [1, 30, 56]. The magnetic field dependence MR (%) at constant temperatures of 5 and 300 K are shown in Fig. 9a, b for BFGMO samples. It is understood from Fig. 9a, b that the magnitude of MR (%) raises with an increase of magnetic field at constant temperatures of 5 and 300 K, is owing to the lowering of spin scattering at grain boundaries in the presence of magnetic field. This enhancement of MR (%) with magnetic field occurs below Curie temperature of the samples, where the polarization of carriers is large [16, 38, 52, 53, 55–57].

The values of MR (%) at 1 T, and 5 and 300 K, are obtained from Fig. 9a, b and given in Table 3. It is noticed from Table 3 that the values of MR (%) enhanced by varying the Ga in BFGMO at 5 K. The increase in MR (%) with Ga in BFGMO sample is due to the weakening of the double exchange barrier after Ga doping in Ba_2FeMoO_6 samples [26, 33, 38, 55, 58]. In such a case, for electron transport along the chain in the ferromagnetic segregation Ga ions may act as a barrier and weaken the ferromagnetic exchange.

It is found from Fig. 9a that low-field magneto-resistance has occurred for BFGMO samples. The value of LFMR (%) for composition x = 0.3 is largest, i.e., 10.62% at 1 T and 5 K compared to other samples in BFGMO

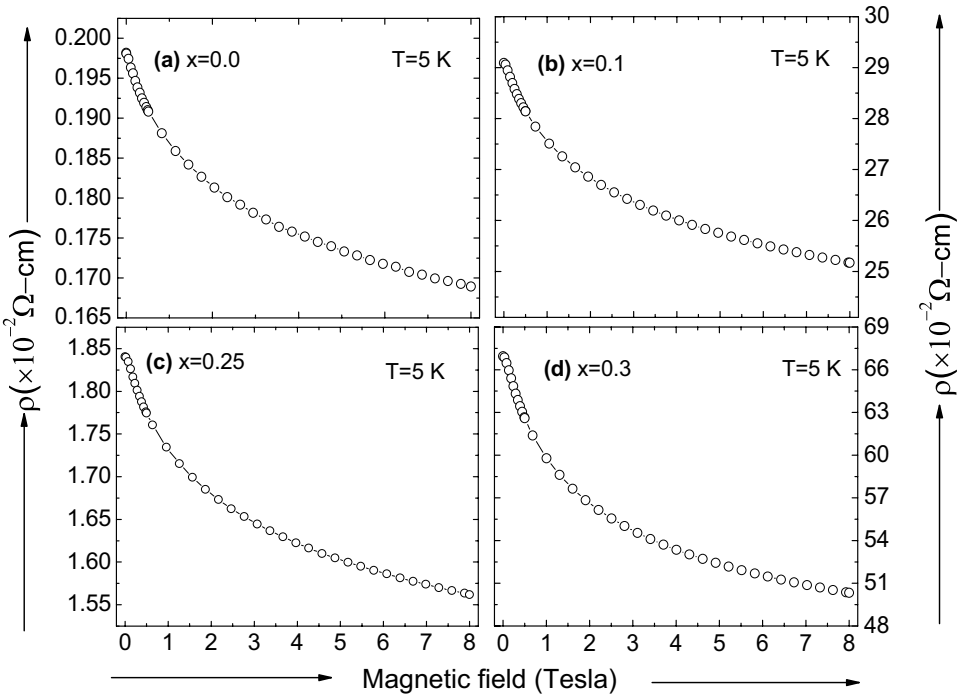

Fig. 6 (**a**–**d**) Variation of resistivity with magnetic field range from 0 to 8 T of $Ba_2Fe_{1-x}Ga_xMoO_6$ at constant temperature 5 K for composition (**a**) x = 0.0, (**b**) x = 0.1, (**c**) x = 0.25 and (**d**) x = 0.3

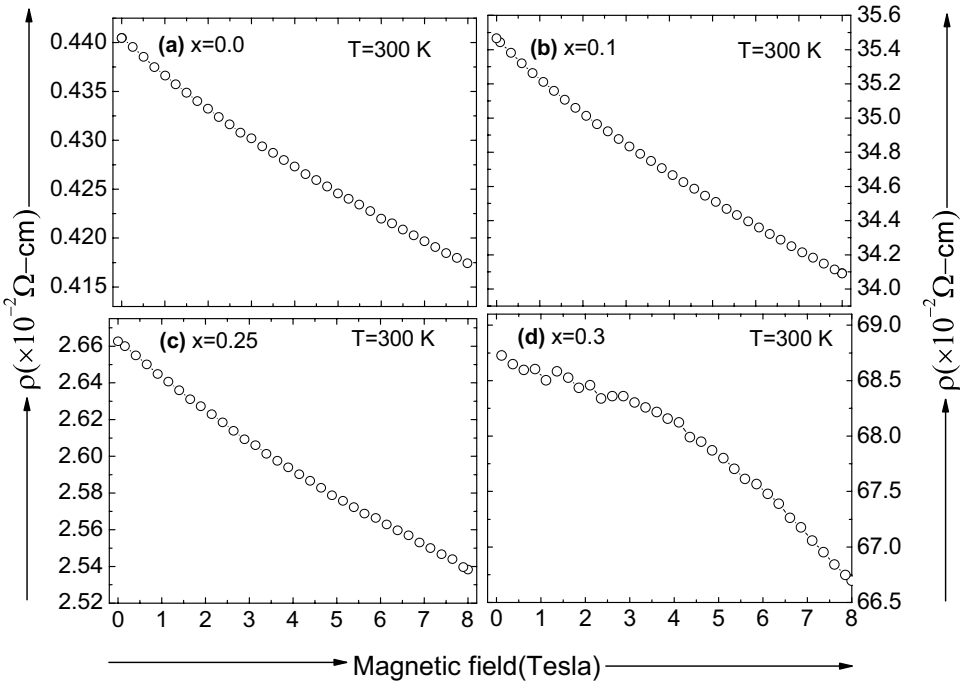

Fig. 7 (**a**–**d**) Variation of resistivity with magnetic field range from 0 to 8 T of $Ba_2Fe_{1-x}Ga_xMoO_6$ at constant temperature 300 K for composition (**a**) x = 0.0, (**b**) x = 0.1, (**c**) x = 0.25 and (**d**) x = 0.3

series. In the double perovskite systems, magneto-resistance response originates from tunneling of spin-polarized charge carriers through insulating barriers. These barriers may be Fe–Mo disorder defects, grain boundaries (giving inter-granular magneto-resistance), and some domain boundaries (giving intra-granular magneto-resistance) [4, 16, 38, 55]. Spin polarization of charge carriers plays an important role in both of these tunneling magneto-resistance. The high magnetic softness of the material is also important as it increases the magnetic field response of magneto-resistance. The similar LFMR results had been reported by Liu at al [26] at 5 K and magnetic field range

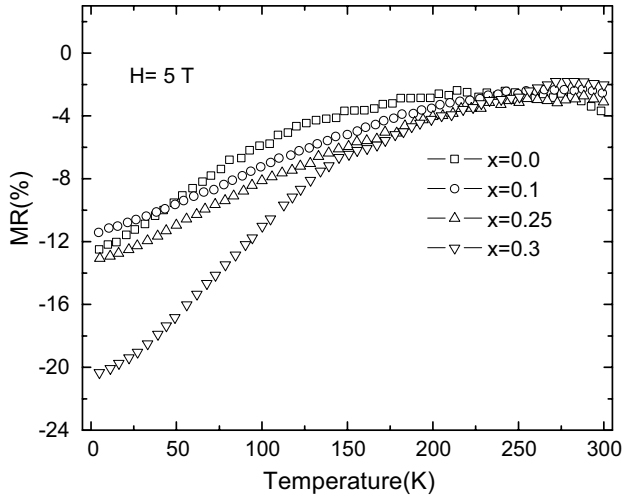

Fig. 8 Variation of MR (%) with temperature from 5 to 300 K of $Ba_2Fe_{1-x}Ga_xMoO_6$ (x = 0.0, 0.1, 0.25 and 0.3) samples at constant magnetic field 5 T

0–2 T in $Sr_2Fe_{1-x}Ga_xMoO_6$ samples. The spin polarization in the double perovskite systems is very sensitive to temperature and to anti-site defects (ASDs). It is observed from Table 3 that the MR (%) decreases with the addition of Ga in Ba_2FeMoO_6 at temperature 300 K. It is ascribed to an increase in anti-site defects or a decrease of spin polarization of charge carriers [16, 30, 33, 38, 47, 49, 55, 56]. The MR (%) of the samples depends on various parameters like as temperature, magnetic field and grain boundary effect (grain size). (MR%) of the material is defined as $MR(\%) = \{[\rho(H,T) - \rho(0,T)]/\rho(0,T)\} \times 100$, where ρ(0,T) and ρ(H,T) are the resistivities at zero magnetic field and H magnetic field at temperature T respectively. The value change of resistivity with magnetic field and without magnetic field reduces at room temperature may be attributed to increase of grain boundaries (decrease of grain size) by addition of Ga content. Since MR (%) decreases with Ga content at room temperature due to increase of grain boundaries are one of the reason.

4 Conclusions

The authors studied the structure, charcterization, resistivity and magnetoresistance of the $Ba_2Fe_{1-x}Ga_xMoO_6$ ($0 \le x \le 0.3$) double perovskite materials. The value of lattice parameter decreases with increase in Ga content in BFGMO. FTIR spectra of BFGMO samples showed three characteristic absorption bands between 860–400 cm^{-1} indicating formations of double perovskite structure. It was found from results at room temperature that the value of MR (%) decreased by doping of Ga in the BFGMO samples. The enhancement of MR (%) in the magnetic field range 0–8 T occurred by addition of Ga-content at temperature of 5 K in the BFGMO series. The largest value of LFMR (%), i.e. 10.62%, obtained at 1 T and 5 K for composition x = 0.3 in BFGMO series. The value of MR (%) of BFGMO samples increases with increases of composition at low temperature (5 K) while these values decreases with composition at room temperature (300 K). Novelty of the present work is that the opposite trend is followed in variation of MR (%) with composition at temperature 5 and 300 K in the BFGMO samples.

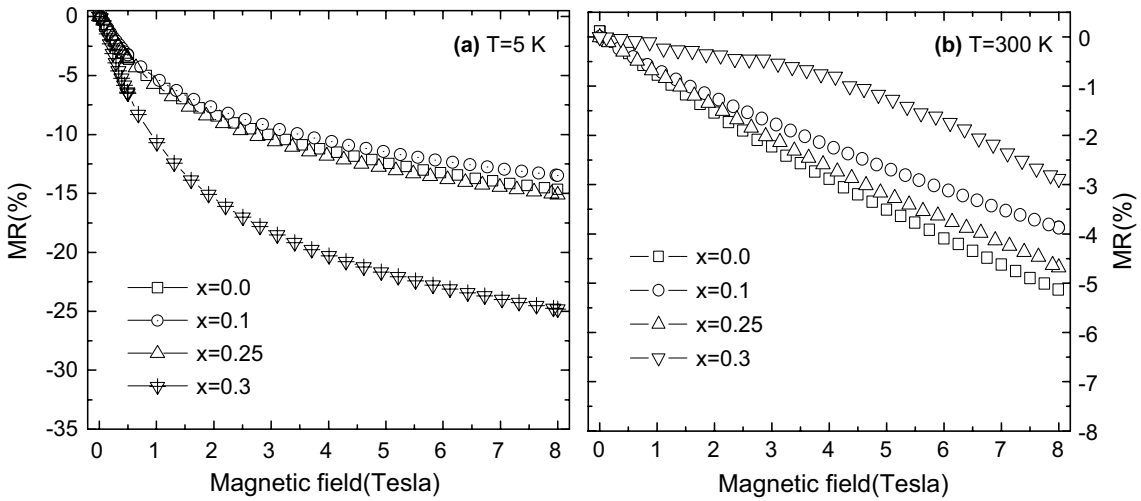

Fig. 9 (**a**, **b**) Variation of MR (%) with magnetic field range from 0 to 8 T at constant temperature (**a**) T = 5 K and (**b**) T = 300 K for $Ba_2Fe_{1-x}Ga_xMoO_6$ (x = 0.0, 0.1, 0.25 and 0.3) samples

Acknowledgements The authors thank Dr. Rajeev Rawat of UGC-DAE, Consortium for Scientific Research, Indore for providing magnetoresistance facilities. The authors acknowledge Department of Science and Technology, New Delhi, India for providing financial assistance to carry out this work under the research project (File No.SB/S2/CMP-004/2013). The authors thank to Dr. N. Venkateshwarlu, Asst. Professor, University College of Law, Prof. S. Ramchandram, Vice Chancellor, Osmania University, Head, Department of Physics, University College of Science, Principal, Nizam College, Osmania University, Hyderabad, India for his encouragement and providing necessary facilities.

References

1. K.I. Kobayashi, T. Kimura, H. Sawada, K. Terakura, Y. Tokura, Nature **395**, 677 (1999)
2. A. Maignan, B. Raveau, C. Martin, M. Hervieu, J. Solid State Chem. **144**, 224 (1999)
3. H.Y. Hwang, S.W. Cheong, N.P. Ong, B. Batlog, Phys. Rev. Lett. **77**, 2041 (1996)
4. D.D. Sarma, S. Ray, K. Tanaka, M. Kobayashi, A. Fujimori, P. Sanyal, H.R. Krishnamurthy, C. Dasgupta, Phys. Rev. Lett. **98**, 157205 (2007)
5. H.F. Zhao, L.P. Cao, Y.J. Song, S.M. Feng, X. Shen, X.D. Ni, Y. Yao, Y.G. Wang, Solid State Commun. **204**, 1–4 (2015)
6. D.D. Sarma, Curr. Opin. Solid State Mater. Sci. **5**, 261 (2001)
7. S.B. Kim, B.W. Lee, S.R. Yoon, C.S. Kim, J. Magn. Magn. Mater. **245–255**, 580–582 (2003)
8. Q. Zhang, Z.F. Xu, J. Liang, J. Pei, H.B. Sun, J. Magn. Magn. Mater. **354**, 231–234 (2014)
9. V. Pandey, V. Verma, R.P. Aloysius, G.L. Bhalla, V.P.S. Awana, H. Kishan, R.K. Kotnala, J. Magn. Magn. Mater. **321**, 2239–2244 (2009)
10. H. Han, B.J. Han, J.S. Park, B.W. Lee, S.J. Kim, C.S. Kim, J. Appl. Phys. **89**, 7687 (2001)
11. A.S. Ogale, S.B. Ogale, R. Ramesh, T. Venkatesan, Appl. Phys. Lett. **75**, 537 (1999)
12. T. Goko, Y. Endo, E. Morimoto, J. Arai, T. Matsumoto, Phys. B **333–329**, 837–839 (2003)
13. H. Han, C.S. Kim, B.W. Lee, J. Magn. Magn. Mater. **254–255**, 574–576 (2003)
14. W.Y. Lee, H. Han, S.B. Kim, C.S. Kim, B.W. Lee, J. Magn. Magn. Mater. **254–255**, 577–579 (2003)
15. A.G. Floresa, M. Zazo, J. Íñiguez, V. Raposo, C. de Francisco, J.M. Muñoz, W.J. Padilla, J. Magn. Magn. Mater. **254–255**, 583–585 (2003)
16. M. García-Hernández, J.L. Martínez, M.J. Martínez-Lope, M.T. Casais, J.A. Alonso, Phys, Rev.Lett **86**, 2443 (2001)
17. F.K. Patterson, C.W. Moeller, R. Ward, Inorg, Chem **29**, 196 (1963)
18. M. Itoh, I. Ohta, Y. Inaguma, Mater. Sci. Eng. B **41**, 55 (1996)
19. E.K. Hemery, G.V.M. Williams, H.J. Trodahl, Curr. Appl. Phys. **6**, 312–315 (2006)
20. H.M. Yang, H. Han, B.W. Lee, J. Magn. Magn. Mater. **272–276**, 1831–1833 (2004)
21. Q. Zhang, G.H. Rao, H.Z. Dong, Y.G. Xiao, X.M. Feng, G.Y. Liu, Y. Zhang, J.K. Liang, Phys. B **370**, 228–235 (2005)
22. V. Pandey, V. Verma, R.P. Aloysius, G.L. Bhalla, R.K. Kotnala, Solid State Commun. **149**, 869–873 (2009)
23. X.M. Feng, G.H. Rao, G.Y. Liu, W.F. Liu, Z.W. Ouyang, J.K. Liang, J. Phys. Condens. Matter **16**, 1813–1821 (2004)
24. J. Kim, J.G. Sung, H.M. Yang, B.W. Lee, J. Magn. Magn. Mater. **290–291**, 1009–1011 (2005)
25. K. Ramesh, A.S. Prakash, Mater. Sci. Eng., B **164**, 124–130 (2009)
26. M.F. Lu, J.P. Wang, J.F. Liu, W. Song, X.F. Hao, De F. Zhou, X.J. Liu, Z.J. Wu, J. Meng. J. Alloys Compd. **428**, 214–219 (2007)
27. Y. Markandeya, D. Saritha, M. Vithal, A.K. Singh, G. Bhikshamaiah, J. Alloys Compd. **509**, 5195–5199 (2011)
28. Y. Markandeya, K. Suresh, G. Bhikshamaiah, J. Alloys Compd. **509**, 9598–9603 (2011)
29. S. Ferau, P. Samoila, A.I. Borhan, M. Ignat, A.R. Iordan, M.N. Palamaru, Mater. Charact. **84**, 112–119 (2013)
30. Y. Markandeya, Y. Suresh Reddy, S. Bale, G. Bhikshamaiah, J. Mater. Sci.: Mater. Electron. **29**, 6711–6719 (2018)
31. Y. Suresh Reddy, Y. Markandeya, B. Appa Rao, G. Bhikshamaiah, J. Mater. Sci.: Mater. Electron. **29**, 2966–2973 (2018)
32. Y. Markandeya, Y. Suresh Reddy, S. Bale, C. Vishnuvardhan Reddy, G. Bhikshamaiah, J. Bull. Mater Sci **38**, 1603–1608 (2015)
33. Y. Markandeya, Y. Suresh Reddy, A. Manjula Devi, K. Suresh, G. Bhikshamaiah, IOP Conf. Ser.: J. Mater. Sci. Eng. **73**, 012097 (2015)
34. G. Rajender, Y. Markandeya, A.K. Singh, G. Bhikshamaiah, IOP Conf. Ser.: J. Mater. Sci. Eng. **330**, 012007 (2018)
35. S. Varaprasad. K. Thyagarajan. Y. Markandeya, K. Suresh, G. Bhikshamaiah J. Mater. Sci.: Mater. Electron. (2018). https://doi.org/10.1007/s10854-018-9488-z
36. S. Varaprasad, K. Thyagarajan, Y. Markandeya, K. Suresh, G. Bhikshamaiah J. Supercond. Nov. Magn. (2018). https://doi.org/10.1007/s10948-018-4738-0
37. H.-E.M.M. Saad, N. Rammeh, Phys. B **481**, 217–223 (2016)
38. S. Vasala, M. Karppinen, J. Prog. Solid State Chem. **43**, 1–36 (2015)
39. J.H. Kim, G.Y. Ahn, S.-I. Park, C.S. Kim. J. Magn. Magn. Mater. **282**, 295–298 (2004)
40. X.M. Feng, G.H. Rao, G.Y. Liu, H.F. Yang, W.F. Liu, Z.W. Ouyang, J.K. Liang, Phy. B **344**, 21–26 (2004)
41. L. Vegard, Die Konstitution der Mischkristalle und die Raumfüllung der Atome. Zeitschrift für Physik **5**, 17–26 (1921)
42. T. Tiittannen, M. Karppinen, J. Solid State Chem. **246**, 245–251 (2017)
43. R.D. Shannon, C.T. Prwitt, Acta Cryst. B **25**, 925–946 (1969)
44. D.A.L. Tellez, D.P. Llamosa, C.E.D. Toro, A.V.G. Rebaza, J. Roa-Rojas, J. Mol. Struct. **1034**, 233–237 (2013)
45. M.F. Mostafa, S.S. Ata-Allah, A.A.A. Youssef, H.S. Refai, J. Magn. Magn. Mater **320**, 344 (2008)
46. A.E. Lavat, E.J. Baran, Vib. Spectrosc. **32(2)**, 167 (2003)
47. L. Harnagea, P. Berthet, J. Solid State Chem. **222**, 112–115 (2015)
48. B. Ufacial, C. Adriano, R. Lora-Serrano, J.G.S. Duque, L. Mendovca-Ferreira, C. Rojas-Ayala, E. Baggio-Saitovitch, E.M. Bittar, P.G. Pagliuso, J. Solid State Chem. **212**, 23–29 (2014)
49. Y. Lan, X. Feng, X. Zhang, Y. Shen, D. Wang, Phys. Lett. A **380**, 2962–2967 (2016)
50. M. Khlifi, M. Wali, E. Dhahri, J. Phys. B **449**, 36–41 (2014)
51. E.K. Hemery, G.V.M. Williams, H.J. Throdahl, Phys. B **394**, 74–80 (2007)
52. F. Sher, A. Venimadhav, M.G. Blamire, B. Dabrowski, S. Kolesnik, J.P. Attfield, Solid State Sci. **7**, 912–919 (2005)
53. A. Dhahri, M. Jemmali, E. Dhahri, E.K. Hlil, J. Dalton Trans. **44**, 620 (2015)
54. Y.-Q. Zhai, J. Qiao, Z. Zhang, E-J. Chem. **8**(S1), S189–S194 (2011)
55. D. Serrate, J.M. De Teresa, P.A. Algarabel, J. Galibert, C. Ritter, J. Blasco, M.R. Ibarra, Phys. Rev. B **75**, 165109 (2007)
56. A. Gaur, G.D. Varma, H.K. Singh, J. Alloy. Compd. **460**, 581–584 (2008)
57. F. Sher, A. Venimadhav, M.G. Blamire, K. Kamenev, J.P. Attifield, Chem. Mater. **17**, 176 (2005)
58. Y. Sui, X.J. Wang, Z.N. Qian, J.G. Cheng, Z.G. Liu, J.P. Miao, Y. Li, W.H. Su, C.K. Ong, Appl. Phys. Lett. **85**, 269 (2004)